ENVIRONMENTAL RESEARCH
LETTERS

LETTER • OPEN ACCESS

Data-driven quantification of nitrogen enrichment impact on Northern Hemisphere plant biomass

To cite this article: Yongwen Liu *et al* 2022 *Environ. Res. Lett.* **17** 074032

View the article online for updates and enhancements.

You may also like

- Exploring the Origins of Earth's Nitrogen: Astronomical Observations of Nitrogen-bearing Organics in Protostellar Environments
Thomas S. Rice, Edwin A. Bergin, Jes K. Jørgensen et al.

- THE VERY MASSIVE STAR CONTENT OF THE NUCLEAR STAR CLUSTERS IN NGC 5253
L. J. Smith, P. A. Crowther, D. Calzetti et al.

- ISOTOPIC ANOMALIES IN PRIMITIVE SOLAR SYSTEM MATTER: SPIN-STATE-DEPENDENT FRACTIONATION OF NITROGEN AND DEUTERIUM IN INTERSTELLAR CLOUDS
Eva S. Wirström, Steven B. Charnley, Martin A. Cordiner et al.

This content was downloaded from IP address 2.57.131.129 on 10/08/2022 at 11:57

IOP Publishing Environ. Res. Lett. 17 (2022) 074032 https://doi.org/10.1088/1748-9326/ac7b38

ENVIRONMENTAL RESEARCH
LETTERS

CrossMark

OPEN ACCESS

RECEIVED
30 April 2022

REVISED
17 June 2022

ACCEPTED FOR PUBLICATION
22 June 2022

PUBLISHED
6 July 2022

Original content from this work may be used under the terms of the Creative Commons Attribution 4.0 licence.

Any further distribution of this work must maintain attribution to the author(s) and the title of the work, journal citation and DOI.

LETTER

Data-driven quantification of nitrogen enrichment impact on Northern Hemisphere plant biomass

Yongwen Liu[1], Shilong Piao[1,2,*], David Makowski[3], Philippe Ciais[4], Thomas Gasser[5], Jian Song[6], Shiqiang Wan[6], Josep Peñuelas[7,8] and Ivan A Janssens[9]

[1] State Key Laboratory of Tibetan Plateau Earth System, Resources and Environment (TPESRE), Institute of Tibetan Plateau Research, Chinese Academy of Sciences, Beijing 100101, People's Republic of China
[2] Sino-French Institute for Earth System Science, College of Urban and Environmental Sciences, Peking University, Beijing 100871, People's Republic of China
[3] Université Paris-Saclay, AgroParisTech, INRAE, Unit Applied Mathematics and Computer Science (MIA 518), Palaiseau, France
[4] Laboratoire des Sciences du Climat et de l'Environnement, CEA-CNRS-UVSQ, Gif-sur-Yvette 91191, France
[5] International Institute for Applied Systems Analysis (IIASA), 2361 Laxenburg, Austria
[6] College of Life Sciences, Hebei University, Baoding, Hebei 071002, People's Republic of China
[7] CREAF, Cerdanyola del Valles, Barcelona 08193, Catalonia, Spain
[8] CSIC, Global Ecology Unit CREAF- CSIC-UAB, Bellaterra, Barcelona 08193, Catalonia, Spain
[9] Department of Biology, University of Antwerp, Universiteitsplein 1, 2610 Wilrijk, Belgium
[*] Author to whom any correspondence should be addressed.

E-mail: slpiao@pku.edu.cn

Keywords: field experiment, nitrogen deposition, carbon cycle, machine-learning, ecosystem process model

Supplementary material for this article is available online

Abstract

The production of anthropogenic reactive nitrogen (N) has grown so much in the last century that quantifying the effect of N enrichment on plant growth has become a central question for carbon (C) cycle research. Numerous field experiments generally found that N enrichment increased site-scale plant biomass, although the magnitude of the response and sign varied across experiments. We quantified the response of terrestrial natural vegetation biomass to N enrichment in the Northern Hemisphere (>30° N) by scaling up data from 773 field observations (142 sites) of the response of biomass to N enrichment using machine-learning algorithms. N enrichment had a significant and nonlinear effect on aboveground biomass (AGB), but a marginal effect on belowground biomass. The most influential variables on the AGB response were the amount of N applied, mean biomass before the experiment, the treatment duration and soil phosphorus availability. From the machine learning models, we found that N enrichment due to increased atmospheric N deposition during 1993–2010 has enhanced total biomass by 1.1 ± 0.3 Pg C, in absence of losses from harvest and disturbances. The largest effect of N enrichment on plant growth occurred in northeastern Asia, where N deposition markedly increased. These estimates were similar to the range of values provided by state-of-the-art C–N ecosystem process models. This work provides data-driven insights into hemisphere-scale N enrichment effect on plant biomass growth, which allows to constrain the terrestrial ecosystem process model used to predict future terrestrial C storage.

1. Introduction

In the last century, humans have drastically altered the global nitrogen (N) cycle by producing reactive N and spreading it over ecosystems. Reactive N inputs come from fertilizers synthesis by the Haber–Bosch process, N oxides produced by fossil fuels and biofuels, and the cultivation of N_2-fixing crops (Vitousek *et al* 1997, Galloway *et al* 2004, 2008, Canfield *et al* 2010, Peñuelas *et al* 2020). Here we focus on the impact of increasing N deposition (Dentener *et al* 2006, Ackerman *et al* 2019), on terrestrial ecosystems (Hietz *et al* 2011, Fowler *et al* 2013). Previous studies found that most

© 2022 The Author(s). Published by IOP Publishing Ltd

terrestrial ecosystems were limited by N availability, particularly in the Northern Hemisphere at mid- and high latitudes (Elser *et al* 2007, LeBauer and Treseder 2008, Peñuelas *et al* 2013, Craine *et al* 2018, Du *et al* 2020). Clarifying the effect of atmospheric N input on the growth of terrestrial plants is thus critical to understand terrestrial carbon (C) storage, i.e. how much of the current land C sink is caused by atmospheric deposition (Gruber and Galloway 2008, Reay *et al* 2008, Schulte-Uebbing *et al* 2022).

Field N-enrichment experiments have been conducted in various terrestrial ecosystems during the last four decades (figure 1(a)). The data from such site-scale field experiments were and continue to be used to explore the effects of N enrichment on ecosystem C cycling (LeBauer and Treseder 2008, Janssens *et al* 2010, Song *et al* 2019, Du *et al* 2020). For instance, meta-analyses of N-enrichment experiments showed that the mean effect of N enrichment on site-scale biomass was positive (LeBauer and Treseder 2008, Yue *et al* 2017, Schulte-Uebbing and de Vries 2018, Song *et al* 2019). However, the effect of N enrichment on biomass varies drastically across experiments, due to local conditions such as climate, vegetation, background soil fertility, N-enrichment intensity and duration, and experimental design (Xia and Wan 2008, Stewart 2010, Greaver *et al* 2016). This large variability poses a substantial challenge to the data-driven quantification of regional- or global-scale responses of terrestrial biomass to elevated N deposition.

We quantified the effects of climate, soil characteristics, and N-enrichment intensity on the response of Northern Hemisphere vegetation biomass to N enrichment using two machine-learning algorithms. Given that there may be divergence in plant above- and below-ground adjustment strategies under resource stress (Freschet *et al* 2018, Tumber-Dávila *et al* 2022), we investigated the dominant source of variation in N enrichment effects in both aboveground biomass (AGB) and belowground biomass (BGB). The machine-learning algorithms were trained using data from peer-reviewed N-enrichment experimental studies (see Methods). In total, we compiled 597 observations of the response of AGB to N addition from 100 sites, and 176 observations of the response of BGB from 42 sites (table S1, supplementary data). All the N-enrichment experiments were paired with a control and a treatment at the same location. The AGB and BGB responses cumulate effects of N addition throughout the experimental period.

The data on AGB and BGB responses covered a range of vegetation types (figure 1(a) and table S1) and intensity of N enrichment from 0.2 to 64 g N m^{-2} y^{-1} at AGB sites (figure 1(b)) and from 1 to 56 g N m^{-2} y^{-1} at BGB sites (figure 1(c)). The atmospheric N deposition change during 1993–2010 reaches at highest 1.3 g N m^{-2} y^{-1} (figure 1(a)). Thus, N enrichment intensity in the experiments somewhat covered the change in atmospheric N deposition, albeit with a significant bias towards the higher end and beyond. In this study, in addition to meta-analyses approach, we used boosted regression trees (BRT) (Elith *et al* 2008) and random forest (RF) models (Breiman 2001) to predict the responses of AGB and BGB to the intensity of N-enrichment. The conclusions from the two machine-learning algorithms were consistent, so we present the results obtained with BRT in the main text (and the RF results in supplementary information).

2. Methods

2.1. Data set of N-enrichment experiments

We collected data for AGB and BGB in N-enrichment experiments from four meta-analyses: Song *et al* (2019), Schulte-Uebbing and de Vries (2018), Yue *et al* (2017), and Tian *et al* (2016). We obtained the data in Song *et al* (2019) from the authors and the data in the other three studies that were not included in Song *et al* (2019) from references provided therein. We used data from N-enrichment experiments in natural terrestrial ecosystems between 30–90° N. The median experimental duration was three years (figure S1). We collected a total of 597 records (including replicates and years in each site) for the response of AGB to N addition from 100 sites and a total of 176 records (including replicates and years in each site) for the response of BGB from 42 sites (table S1, figure 1(a), supplementary data).

2.2. Meta-analysis of observed effects of N enrichment on above- and belowground biomass

The effect of N enrichment on AGB (or BGB) likely varies across the N-enrichment experiments due to the spatial heterogeneity in climatic, soil, and experimental characteristics. Thus, in the meta-analysis, we used random-effects models assuming that the effects being estimated in the different studies are not identical, but follow some distribution representing the between-study variability (Gurevitch *et al* 2018). We conducted the meta-analysis using the 'escalc' and 'rma.uni' functions in the 'metafor' package of R software (Viechtbauer 2010). Specifically, the effects of N on AGB and BGB were measured by estimating the mean response ratio $RR = \ln\left(\overline{X_t}/\overline{X_c}\right)$, where $\overline{X_t}$ and $\overline{X_c}$ are mean biomasses in the N-enrichment and control treatments, respectively (Hedges *et al* 1999, Lajeunesse 2011). This was performed by setting the parameter 'measure' as 'ROM' in the 'escalc' function in the 'metafor' package of R software (Viechtbauer 2010). The weighted response ratio (RR_w) was calculated as the weighted average of RR using the weights $\omega_i = 1/(\nu_i + \tau^2)$, where ν_i is the variance of the effect size within the ith study and τ^2 is the between-study estimated by a restricted maximum-likelihood estimator (Viechtbauer *et al*

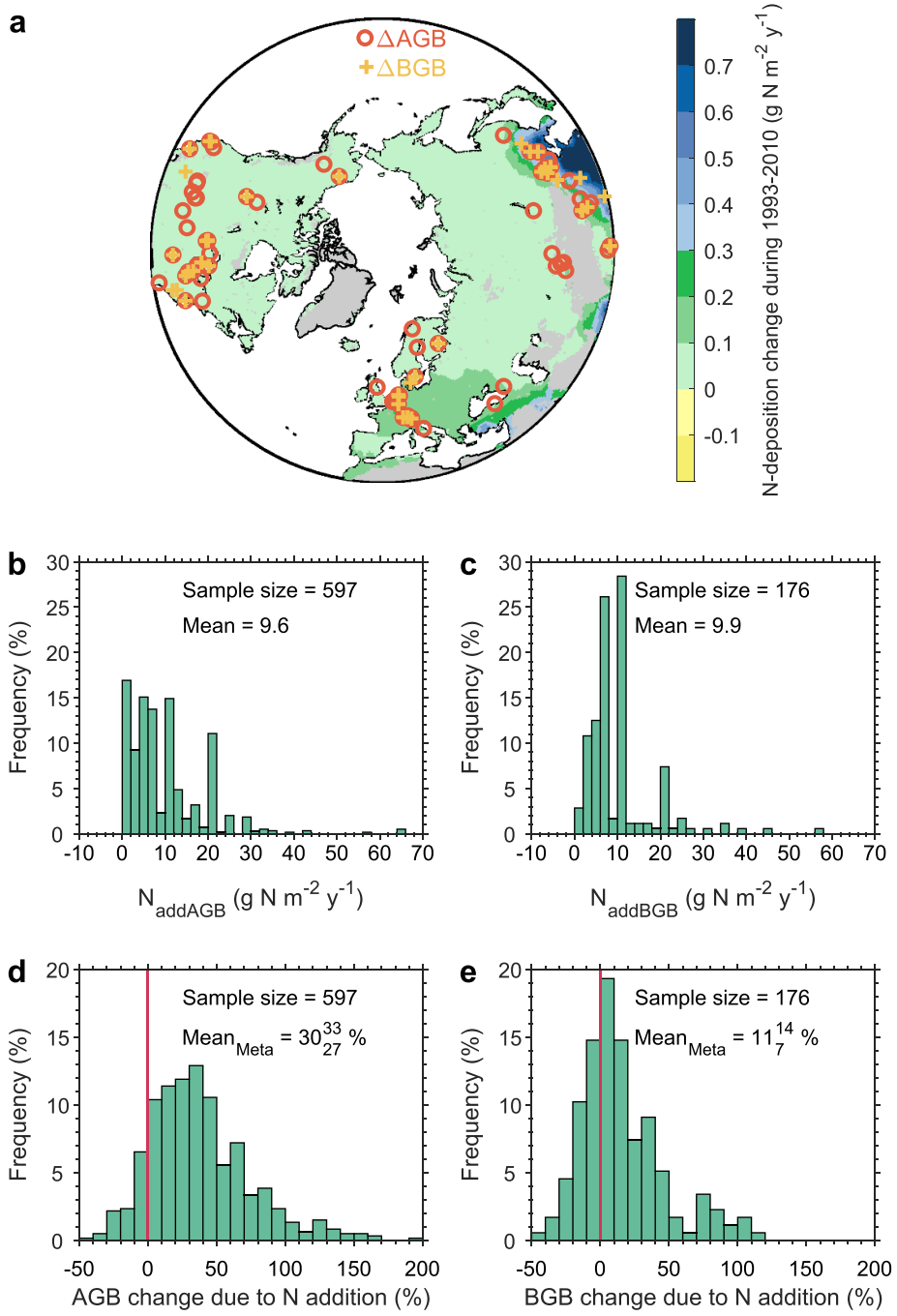

Figure 1. Response of AGB and BGB to N enrichment in N-enrichment experiments. (a) Distribution of the N-enrichment experimental sites with observed AGB and BGB sensitivities (S_{AGB} and S_{BGB}) to N enrichment. Background colors show the changes in N deposition during 1993–2010. (b) and (c) Frequency distribution of amount of N enrichment for observations of AGB and BGB responses (N_{addAGB} and N_{addBGB}). (d) and (e) Frequency distribution of the effect of N enrichment on AGB and BGB. The percent of biomass change (%) is N enrichment-induced relative change in AGB (d) and BGB (e) over the experimental period. The red vertical lines represent nil values. $Mean_{Meta}$ gives the mean and 95% confidence intervals of the effect of N enrichment on AGB and BGB based on the meta-analyses.

2015). Parameter estimation was performed by setting the parameter 'method' as 'REML' in the 'rma.uni' function in the 'metafor' package of R software (Viechtbauer 2010). The percent changes of AGB and BGB due to N enrichment were calculated as $[\exp(RR_w) - 1] \times 100\%$. The effects of N enrichment on AGB and BGB were considered to differ significantly between the N-enrichment and control treatments when the 95% confidence intervals of ΔAGB and ΔBGB did not include zero.

2.3. Observation based sensitivities of AGB and BGB to N enrichment

The sensitivities of AGB and BGB to N enrichment (S_{AGB} and S_{BGB}) were calculated as:

$$S_{AGB} = \frac{\Delta AGB}{N_{add}} \times 100 \quad (1)$$

where S_{AGB} is the relative response of AGB to N enrichment (% [g N m^{-2} $y^{-1}]^{-1}$), ΔAGB is the N enrichment-induced relative change in AGB over the experimental period (%), and N_{add} is the amount of N added in the treatment plots (g N m^{-2} y^{-1}):

$$S_{BGB} = \frac{\Delta BGB}{N_{add}} \times 100 \quad (2)$$

where S_{BGB} is the relative response of BGB to N enrichment (% [g N m^{-2} $y^{-1}]^{-1}$), ΔBGB is the N enrichment-induced relative change in BGB over the experimental period (%), and N_{add} is the amount of N added in the treatment plots (g N m^{-2} y^{-1}).

2.4. Relative influence of climatic, soil, and experimental characteristics on S_{AGB} and S_{BGB}

The spatial variations of S_{AGB} and S_{BGB} were examined using BRT (Elith *et al* 2008) and RF models (Breiman 2001). We conducted the BRT analyses using the 'gbm.step' function in the 'gbm' package of R software, with the parameters of 'tree.complexity' as 5 and 'learning.rate' as 0.005. The RF analyses were conducted using the 'randomForest' function in the 'randomForest' package of R software, with the parameters of 'nodesize' as 5 and 'ntree' as 500. The BRT and RF models were trained using 16 predictor variables: climatic variables (mean annual temperature (MAT) and mean annual precipitation (MAP)), woodiness (woody or nonwoody), foliar N content, soil characteristics (C:N ratio, bulk density, pH (measured in water), cation exchange capacity (CEC), and the contents of organic C, clay, organic phosphorus (P), labile P, and water), and experimental characteristics (AGB and BGB in the control plots, intensity of N addition, and treatment duration). We obtained data for MAT and MAP from the WorldClim2 database (Fick and Hijmans 2017). To ensure the comparability of N deposition data between BRT and RF models and Multi-scale Synthesis and Terrestrial Model Intercomparison Project (MsTMIP) models, we systematically used the same data set for N deposition (Wei *et al* 2014a, 2014b). We extracted data for the soil C:N ratio, bulk density, pH, CEC, and the contents of organic C and clay from the gridded Global Soil Dataset for use in Earth System Models (GSDE) (Shangguan *et al* 2014), and from the WISE30sec database (ISRICWISE) (Batjes 2016). Data for soil-water content were extracted from GSDE (Shangguan *et al* 2014). Data for the contents of soil organic P and labile P were extracted from Global Gridded Soil Phosphorus Distribution Maps at resolutions of 0.5° (Yang *et al* 2014). Data for foliar N content were extracted from global maps of the distributions of plant traits (Butler *et al* 2017). Data for woodiness (woody or nonwoody) were extracted from the Global Mosaics of the standard Moderate Resolution Imaging Spectroradiometer (MODIS) land-cover type data product (MCD12Q1) in the International Geosphere–Biosphere Programme (IGBP) land cover type classification (Friedl *et al* 2010). The forests, shrublands, and woody savannas were defined as 'woody', and the other vegetation types were defined as 'nonwoody'. We used the S_{AGB} and S_{BGB} samples with all 16 variables in the BRT and RF analyses. The data sets for climate, woodiness, N deposition, and soil characteristics were also used in the spatial extrapolation of S_{AGB} and S_{BGB} (figure S2, see below).

The machine learning analysis was performed 100 times to examine the relative influence of each predictor of the 16 predictors on the S_{AGB} and S_{BGB}. Here, relative influence of a predictor in BRT analysis is relative contribution of the variable for a BRT model, which was 'contributions' parameter outputted by 'gbm.step' function in the 'gbm' package of R software. Partial-dependence plots for the variables in BRT models were produced using 'gbm.plot' function. Variable importance in RF analysis was assessed using the total decrease in residual sum of squares from splitting regression tree on the variable, which was 'IncNodePurity' parameter in 'importance' object outputted by 'randomForest' function in the 'randomForest' package of R software. Partial-dependence plots for the variables in RF models were produced using 'partialPlot' function. The 16 predictors were ranked by the value of their influence on the S_{AGB} and S_{BGB} from high to low. Then, a series of machine learning models including 2–16 predictors were established to examine the performance of simpler models. For each machine learning model, 10-fold cross-validation was used to test the proportion of variance of S_{AGB} (or S_{BGB}) explained by S_{AGB} (or S_{BGB}) predicted by the models (R^2). The cross-validation were performed 100 times with the average results shown in the figures. The machine learning model with highest R^2 was used in spatial extrapolation of S_{AGB} and S_{BGB} in the following section.

2.5. Spatial extrapolation of S_{AGB} and S_{BGB}

We calculated the spatial distributions of S_{AGB} and S_{BGB} at mid- and high latitudes (30–90° N) of the Northern Hemisphere using both the BRT and RF models trained by site data and of the gridded climatic and soil variables, with the treatment duration set as 17 years from 1993 to 2010, the intensity of N enrichment as the average change in N enrichment during 1993–2010 relative to 1993, and AGB and BGB in 1993. In the spatial extrapolation analysis, the first year of the treatment duration was set as 1993, because 1993 was the first year of the dataset for global AGB (Liu *et al* 2015) used in this study. The last year of the treatment duration was set as 2010, because 2010 was the last year of the duration of the MsTMIP models' simulations (Wei *et al* 2014a) used in this study. BGB was calculated as AGB multiplied by the BGB:AGB ratio (R_{B2A}) (Liu *et al* 2015), with

the source noted as 'Liu' in the figures. We also used R_{B2A} and total biomass reported by Carvalhais *et al* (2014) to calculate global AGB and BGB, with the source noted as 'Carvalhais' in the figures. The GEOCARBON global forest AGB (Santoro *et al* 2015, Avitabile *et al* 2016) was also used for the spatial extrapolation of S_{AGB} and S_{BGB}, with BGB calculated as AGB multiplied by R_{B2A}, with the source noted as 'GEOCARBON in the figures. The relative changes in terrestrial AGB and BGB caused by N deposition during 1993–2010 (ΔAGB and ΔBGB) were calculated as S_{AGB} and S_{BGB} multiplied by the average change in annual N deposition during 1993–2010 using driver data (N deposition) of MsTMIP (Wei *et al* 2014b).

2.6. Total change in terrestrial biomass due to enhanced atmospheric N deposition during 1993–2010 for each grid point

BRT- and RF-based change in total biomass (ΔTB) were calculated for each grid point using ΔAGB and ΔBGB with AGB and BGB as weights:

$$\Delta TB = \frac{\Delta AGB \times AGB_{1993} + \Delta BGB \times BGB_{1993}}{AGB_{1993} + BGB_{1993}} \times 100\% \quad (3)$$

where ΔTB is the percent change in total biomass due to N enrichment during 1993–2010, ΔAGB is the percent change in AGB due to N enrichment during 1993–2010, ΔBGB is the percent change in BGB due to N enrichment during 1993–2010, AGB_{1993} is AGB in 1993 (g C m^{-2}), and BGB_{1993} is BGB in 1993 (g C m^{-2}).

2.7. Δ*TB* in Northern Hemisphere

ΔTB in Northern Hemisphere (30–90° N) was calculated as:

$$\Delta TB = \frac{\sum_{i=1}^{n}(\Delta TB_i \times TB_{1993,i} \times Area_i)}{TB_{1993NH}} \times 100\%. \quad (4)$$

where ΔTB is the percent change in total biomass due to N enrichment during 1993–2010, i indicates grid cell i (0.5° × 0.5°), n indicates the number of grid cells, ΔTB_i is the percent change in total biomass due to N enrichment during 1993–2010 at grid cell i, TB_{1993i} is total biomass in 1993 at grid cell i (g C m^{-2}), $Area_i$ is the area of grid i (m^2), and TB_{1993NH} is total biomass in 1993 (g C), calculated as $TB_{1993NH} = \sum_{i=1}^{N}(TB_{1993i} \times Area_i)$.

2.8. Terrestrial ecosystem process model simulations

We used total biomass from six terrestrial ecosystem process models with C–N interactions: CLM4, CLM4VIC, DLEM, ISAM, TEM6, and TRIPLEX-GHG from MsTMIP (Huntzinger *et al* 2013, Wei *et al* 2014a). The model CLASS-CTEM-N results indicated that elevated N deposition reduced terrestrial biomass and was not used in this study. We used model outputs for the SG3 and BG1 scenarios. (a) Under scenario SG3, the models were forced by time-varying climate, land-use and land-cover change (LULCC), and CO_2 concentration. (b) Under scenario BG1, the models were forced by time-varying climate, LULCC, CO_2 concentration, and N deposition. Total biomass induced by N deposition was calculated as the difference between the total biomasses under the BG1 and SG3 scenarios.

ΔTB for each grid point in the MsTMIP models was calculated as:

$$\Delta TB = \frac{TB_{2010} - TB_{1993}}{TB_{1993}} \times 100\% \quad (5)$$

where ΔTB is the percent change in total biomass due to N enrichment during 1993–2010, TB_{1993} is total biomass in 1993 (g C m^{-2}) induced by N deposition, and TB_{2010} is total biomass in 2010 (g C m^{-2}) induced by N deposition.

The relative change in Northern Hemisphere plant biomass due to N enrichment the MsTMIP models was calculated using equation (4) as the change in total biomass induced by N deposition during 1993–2010.

3. Results

Meta-analyses of our dataset revealed that N enrichment on average increased both AGB and BGB in field experiments. AGB was higher by $30^{33}_{27}\%$ (mean and 95% confidence interval) (figure 1(d)) and BGB by $11^{14}_{7}\%$ (figure 1(e)) as compared to each control experiment. The dominant factors influencing the sensitivities of AGB and BGB to N enrichment (S_{AGB} and S_{BGB}, the percent of biomass change over the experimental period due to N enrichment, in % [g N m^{-2} $y^{-1}]^{-1}$) were deduced from the machine-learning algorithms. 16 predictor variables were considered (see Methods). Based on these predictors, the BRT models were able to explain 56%–57% of the variance in S_{AGB} and ∼20% of the variance in S_{BGB} based on our leave-one-out cross-validation (figure 2). The lower performance for BGB was probably due to the lower amount of data available for this variable. The ranges of climatic conditions and soil properties at the experimental sites of N addition covered those observed in terrestrial ecosystems at Northern Hemisphere mid- and high latitudes, indicating the representativeness of the climatic and soil conditions at the experimental sites (table S2).

The intensity of N enrichment had the largest influence on S_{AGB} based on the BRT models (figures 2(a) and (b)). S_{AGB} decreased with N enrichment (figures 3(a), (b), S3 and S4) from ∼15% [g N m^{-2} $y^{-1}]^{-1}$) at a N input of

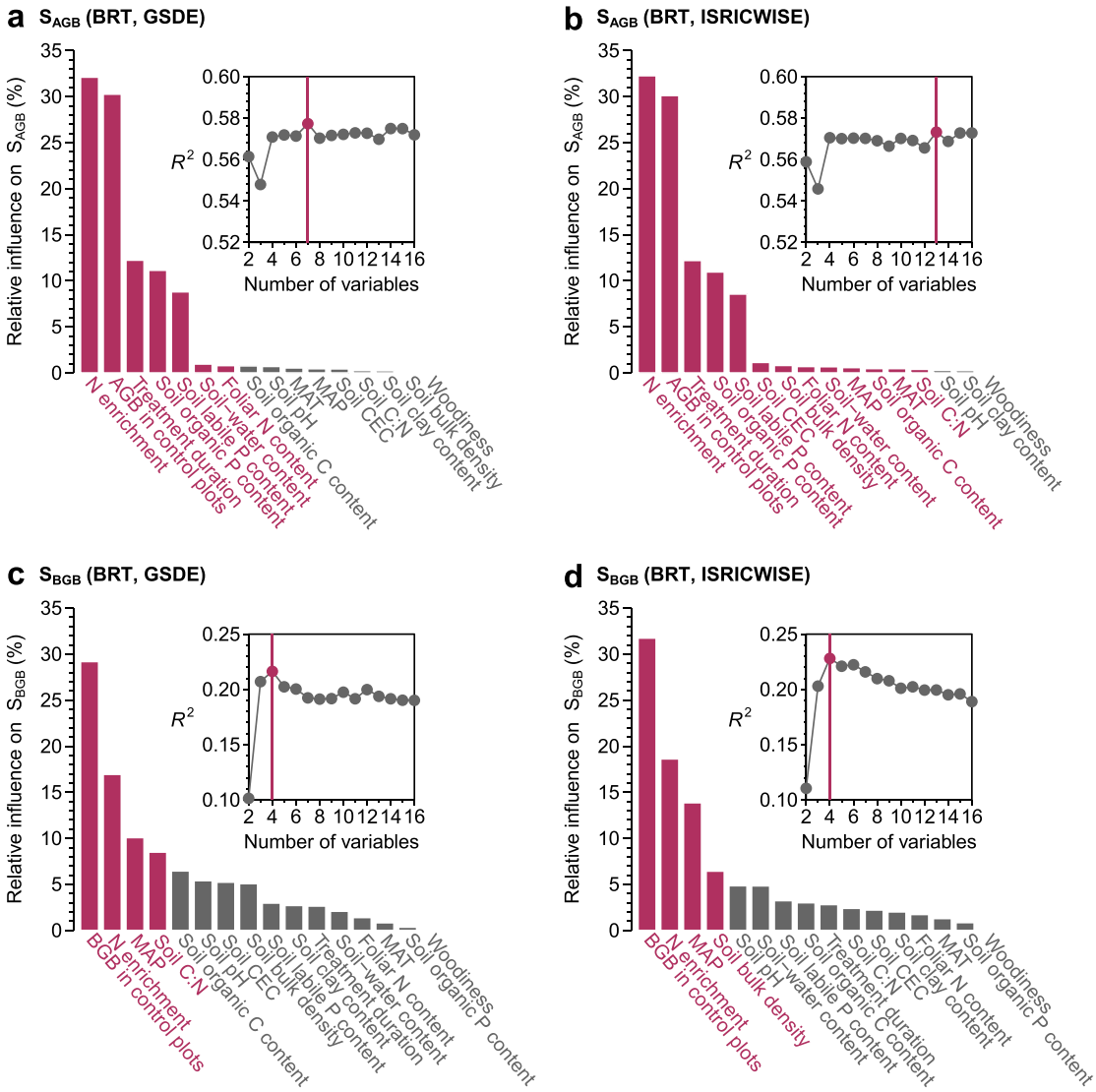

Figure 2. Relative influences of climatic, soil, and experimental characteristics on S_{AGB} and S_{BGB}. (a) and (b) Relative influence on S_{AGB} using BRT, with soil characteristics from the GSDE and ISRICWISE databases, respectively. The relative influence is shown as the mean of the output from 100 BRT analyses. R^2 represents the proportion of variance of S_{AGB} (or S_{BGB}) explained by S_{AGB} (or S_{BGB}) predicted by BRT based on 2–16 predictors. For each BRT model, the cross-validation were performed 100 times with the averaged R^2 shown in the subfigure. The red vertical line shows the BRT model with the largest value of R^2. (c), (d) Same as (a) and (b), but for S_{BGB}.

0.2 g N m^{-2} y^{-1}, to a value close to zero at a very high N input of 64 g N m^{-2} y^{-1}. This was consistent with the results of a regression analysis, which further revealed that S_{AGB} remains close to zero beyond a critical N enrichment intensity of approximately 10 g N m^{-2} y^{-1} (figures S5 and S6). N enrichment intensity was also identified as the largest most influential factor on S_{AGB} by the RF models (figures S7–S9). However, the second most influential factor differed between the two approaches: AGB in the control plot in BRT (figures 2(a), (b), S3 and S4) and soil labile P content (or soil organic P content) in RFs (figures S7–S9).

Unlike S_{AGB}, the dominant source of variation in S_{BGB} was BGB in the control plot (figures 2(c) and (d)), while the intensity of N enrichment was ranked second and also had a strong impact on S_{BGB} (figure S5(c)). S_{BGB} nonlinearly decreased as a function of background BGB (figures 3(c), (d), S5(d), S10, and S11). This result was also evident in the raw observation data (figure S6). The results of the BRT models were generally consistent with those obtained with the RF models results (figures S5, S7, S12 and S13).

In addition to the analysis using all 16 variables, we also performed the analysis with fewer (2–15) variables to establish simpler machine-learning models. BRT models still explained the highest proportion of S_{AGB} variance when using seven most influential variables including soil data from GSDE data set (figure 2(a)) or 13 most influential variables including soil data from ISRICWISE data set (figure 2(b)), and explained S_{BGB} with only four influential variables (figures 2(c) and (d)). This was

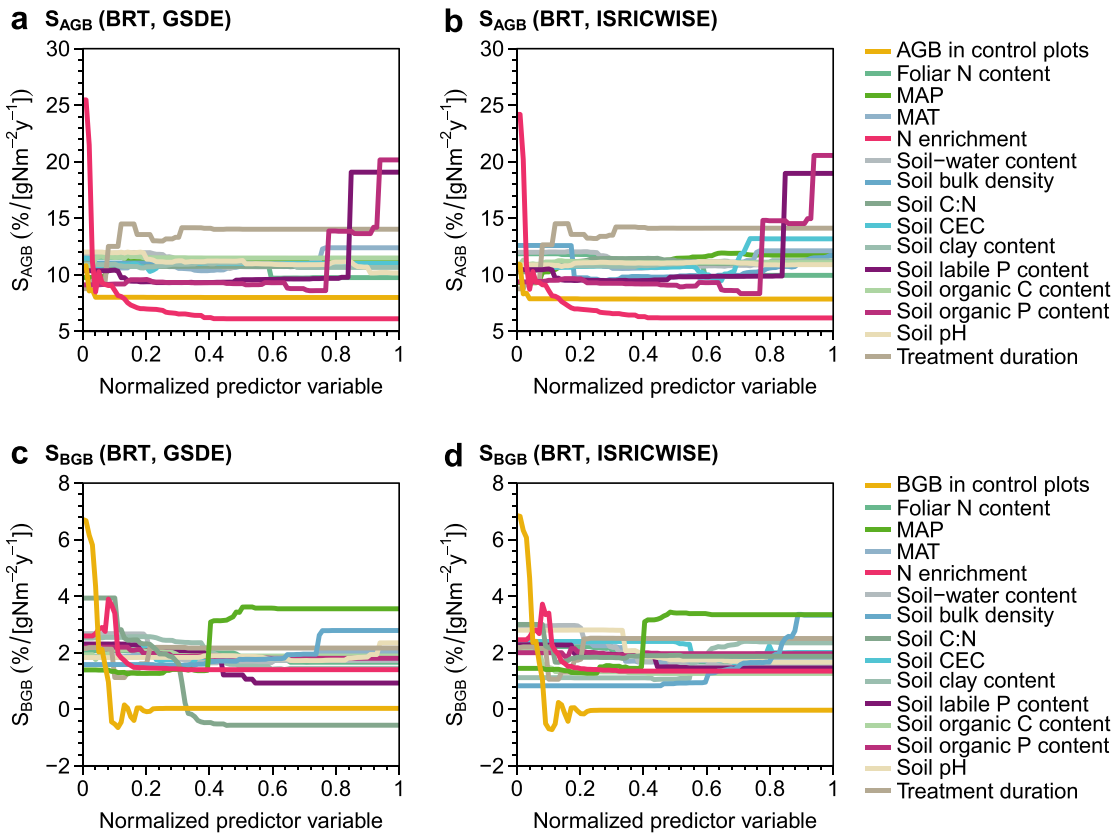

Figure 3. Partial-dependence plots of the predicted S_{AGB} and S_{BGB} with independent predictor variables. (a) and (b) S_{AGB} response to climatic, soil, and experimental variables variation using BRT with soil characteristics from the GSDE and ISRICWISE databases, respectively. The range of predictor variables was normalized to 0–1. (c), (d) Same as a and b, but for S_{BGB}. Figures S3, S4, S10 and S11 show the partial-dependence plots with independent predictor variables expressed as absolute value.

generally consistent with the performance of the RF models (figure S7). Those parsimonious machine-learning models were applied to extrapolate the spatial distributions of S_{AGB} and S_{BGB} across the Northern Hemisphere (>30° N, see Methods). In the extrapolation, the intensity of N enrichment was given by gridded N deposition data during 1993–2010 (Wei *et al* 2014a, 2014b) (figure 1(a)), and the upscaling was calculated for a period of 17 years (1993–2010). The contribution of N enrichment to terrestrial AGB and BGB change (ΔAGB and ΔBGB) were then calculated as S_{AGB} and S_{BGB} multiplied by the average change in annual N deposition during 1993–2010.

The extrapolation analysis shows that AGB generally increased from atmospheric N deposition across the Northern Hemisphere during 1993–2010 (figures 4(a) and S14(a)–(f)), as constrained by observations from the N-enrichment experiments (figure 1(d)). N enrichment had minimal impacts on BGB, but a strong positive effect on AGB changes, that is ΔAGB (figures 4(a), (b) and S14(a)–(l)). This is likely because N enrichment intensity was the most influential factor of the variation of S_{AGB}, but not of S_{BGB}, in the machine-learning models used for upscaling extrapolation. We further analyzed the spatial distribution of the effect of increased N deposition on the change in total biomass (ΔTB) during 1993–2010 by combining the responses of ΔAGB and ΔBGB (Methods). Total biomass was generally enhanced by changes in N deposition across Northern Hemisphere, reflecting the changes in AGB (figures 4(c) and S14(m)–(r)). Biomass increased the most in northeastern Asia, where the largest enhancement of atmospheric N deposition occurred during 1993–2010. The spatial patterns of ΔAGB, ΔBGB, and ΔTB were consistent between the BRT and RF models (figures S14 and S15).

We further investigated ΔTB caused by N enrichment during 1993–2010 using six terrestrial ecosystem process models that include C–N interactions: CLM4, CLM4VIC, DLEM, ISAM, TEM6, and TRIPLEX-GHG from the MsTMIP (Mao *et al* 2015, Huntzinger *et al* 2013, Wei *et al* 2014a). All these models outputted the response of total biomass to N enrichment but did not distinguish between AGB and BGB. None of the models produced the same spatial patterns of ΔTB as those from the machine-learning approaches (figures 4(d) and S16), although the MsTMIP models and the BRT and RF models were all driven by the same N-deposition data set (see methods). The spatial pattern of ΔTB varied greatly

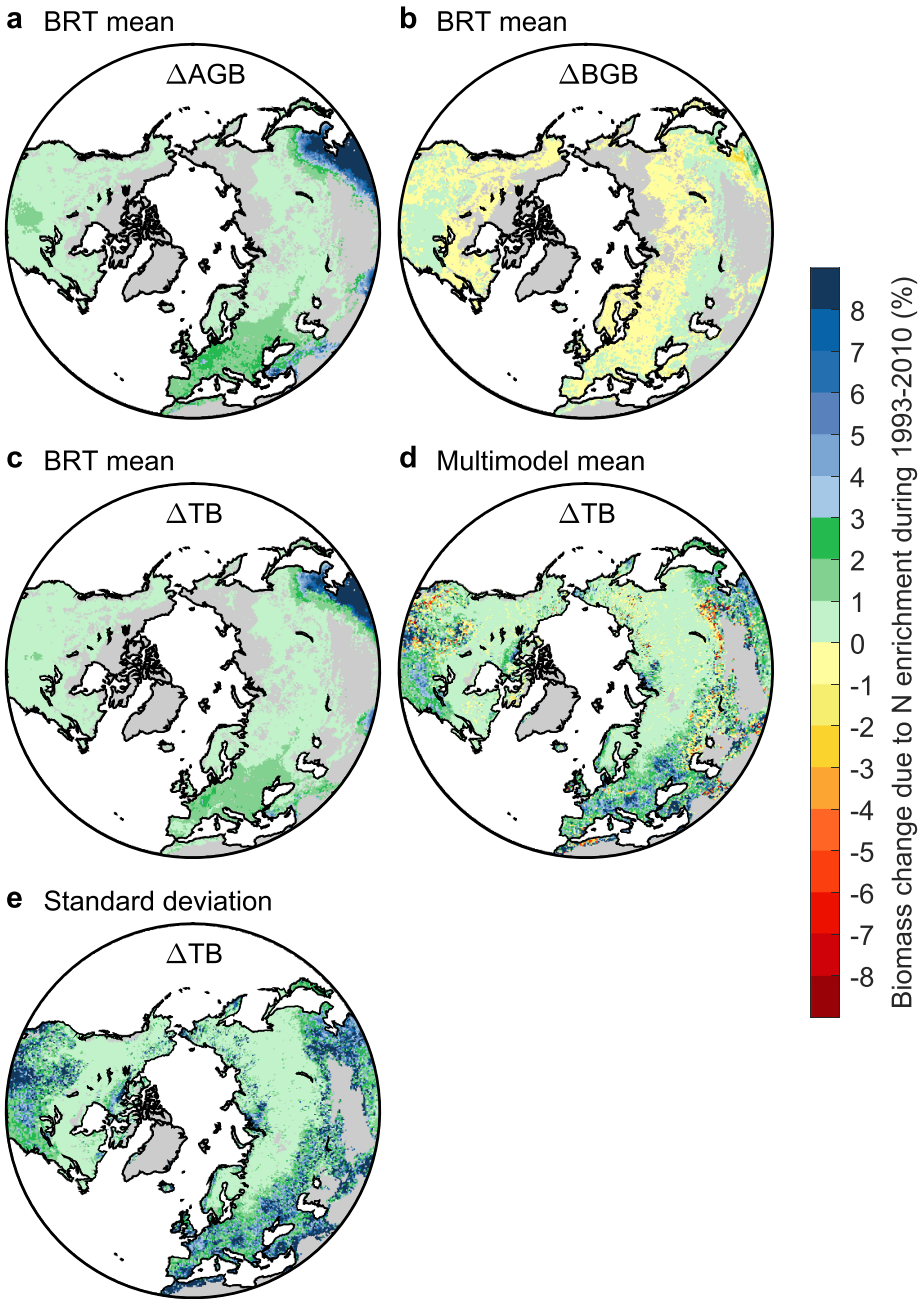

Figure 4. Spatial pattern of relative change in terrestrial biomass due to N enrichment in the Northern Hemisphere during 1993–2010. (a) Mean change in AGB based on BRT. (b), Mean change in BGB based on BRT. (c) Mean change in total biomass based on BRT. The mean spatial patterns in (a)–(c) are the spatial patterns based on BRT using multiple data sources (see figure S14). (d), (e) Multimodel mean, and standard deviation of change in total biomass across the MsTMIP models.

across the six MsTMIP models (figure S16). N enrichment generally had a minimal effect on total biomass in ISAM. Total biomass in the other five models responded positively to N enrichment, albeit to different degrees. The multimodel mean indicated that N enrichment increased total biomass in eastern North America, Europe, and eastern Asia (figures 4(d) and (e)), but with large spread across the terrestrial ecosystem process models (figure S16).

Scaling up spatial values to the entire Northern Hemisphere at mid- and high latitudes, N enrichment during 1993–2010 enhanced total biomass by 0.9 ± 0.3% (1.1 ± 0.3 Pg C) as the average results of the BRT (RF) approach (figures 5 and S17). This increase was dominated by changes in AGB (1.4 ± 0.5%, 1.2 ± 0.3 Pg C, figures S18 and S19) rather than BGB (−0.1 ± 0.1%, −0.04 ± 0.05 Pg C, figures S20 and S21). Relative to the machine learning approaches, ΔTB was underestimated by ISAM (0.0%, 0.0 Pg C) and TRIPLEX-GHG (0.4%, 0.5 Pg C) and was overestimated by CLM4 (1.2%, 1.5 Pg C), CLM4VIC (1.6%, 1.6 Pg C), and DLEM (1.5%, 1.7 Pg C) (figures 5, S17 and table S3). Average ΔTB across the MsTMIP models was 0.9 ± 0.6% (1.2 ± 0.7 Pg C), indicating good agreement between the multi-model mean and our data-driven estimates

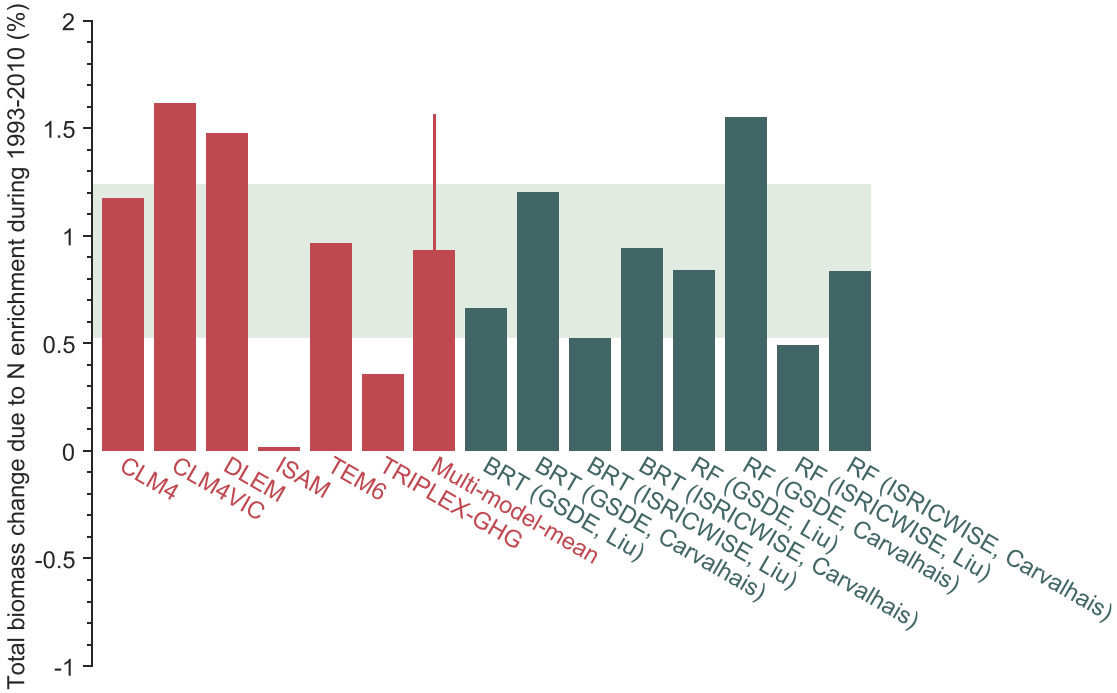

Figure 5. Relative change in terrestrial total biomass caused by N enrichment in the Northern Hemisphere (30–90° N) during 1993–2010. The shaded area shows the mean ± 1 standard deviation of the values based on BRT and RF models. 'Liu' and 'Carvalhais' indicate that the BRT and RF analyses used biomass data from Liu *et al* (2015) and Carvalhais *et al* (2014), respectively.

but also considerable divergence across the state-of-the-art C–N ecosystem models.

4. Discussion and conclusion

Our study based on machine-learning algorithms indicated that the AGB increase responded nonlinearly to the intensity of N addition, consistent with previous meta-analyses (Arens *et al* 2008, Bradford *et al* 2008, Ochoa-Hueso 2016, Tian *et al* 2016, Prager *et al* 2017, Xu *et al* 2018). However, the N enrichment applied in field experiments was typically much higher than the background atmospheric N deposition (figures 1(a)–(c) and S22). Therefore, the overall mean N response estimated by meta-analyses may not accurately represent the larger-scale mean effect of increased N deposition when the strongly nonlinear responses to N addition are not accounted for. In contrast to the meta-analyses, our integrated analyses based on machine-learning approaches did consider the stronger effect of N-enrichment at low doses. The intensity of N enrichment was the dominant cause of terrestrial S_{AGB} variations, when this sensitivity was derived from observations in N-enrichment experiments (figures 2 and S7), with S_{AGB} decreasing from 15% $[g\,N\,m^{-2}\,y^{-1}]^{-1}$ to nearly 0% $[g\,N\,m^{-2}\,y^{-1}]^{-1}$ as N enrichment increased from 0.2 to 64 g N m^{-2} y^{-1}, (figures S3 and S4). The apparent difference in S_{AGB} between our study and previous meta-analyses therefore indicates that considering realistic N enrichment intensity is recommended in future field experiments and meta-analyses studies focusing on N effect on terrestrial C cycling.

Previous meta-analyses have generally suggested positive effects of N addition on AGB (Yue *et al* 2016, You *et al* 2017, Schulte-Uebbing and de Vries 2018) and BGB (Li *et al* 2015, Yue *et al* 2016) in N-enrichment experiments. However, when setting N addition as a change in N deposition during the same duration of 1993–2010 and the identical experimental duration in machine-learning approaches, we found that N enrichment only had a minor effect on Northern Hemisphere terrestrial BGB (figure 4(b)), indicating that N enrichment generally decreased the BGB:AGB ratio in Northern Hemisphere terrestrial ecosystems. This finding is consistent with changes in C allocation due to N enrichment in N-limited terrestrial ecosystems, favoring the allocation of C to AGB instead of roots (Chapin 1980, Müller *et al* 2000, Makela *et al* 2008, Cambui *et al* 2011, Yue *et al* 2021, Peng *et al* 2022). The positive effect of N enrichment on total biomass was dominated by the response of AGB rather than BGB in the Northern Hemisphere terrestrial ecosystems, due to the different responses of AGB and BGB to N enrichment (figures 4(a)–(c)).

N enrichment-induced decrease of the BGB:AGB ratio maybe related to plant adaptation strategies in changing nutrient conditions. Plant biomass allocation changes due to N enrichment were usually

assessed using the two classic mechanisms based on the optimal partitioning hypothesis and the isometric allocation hypothesis, respectively. Under the optimal partitioning hypothesis, biomass is preferentially allocated to the organs that could acquire the most limited resource for plant growth (Bloom *et al* 1985, Kobe *et al* 2010). For instance, plants preferentially allocate more biomass to root under N starvation but allocate more biomass to shoot under N enrichment (Mardanov *et al* 1998, Kobe *et al* 2010, Chen *et al* 2013). Under the isometric allocation hypothesis, the biomass allocation is allometric among plant organs but is isometric across various environmental conditions, plant species or vegetation types (Niklas 2004, 2005). Plants allocate biomass to each organ following scaling exponents based on individual plant size (Cheng and Niklas 2007). The integrated analysis of N enrichment experiments observations showed that N enrichment decreased plant root:shoot ratio but did not apparently change the allometric relationships among plant organs when the whole set of data from various ecosystems were considered (Peng and Yang 2016, Yue *et al* 2021, Peng *et al* 2022). Nevertheless, as shown in figure 5 of Peng *et al* (2022), there was large uncertainty in the allometric scaling exponents among plant organs with 95% confidence interval ranging from ∼0 to ∼2 under both control and N enrichment conditions. Stronger evidence is still needed to clarify whether the allometric relationships are independent of nutrient conditions and vegetation types. Particularly, a higher number of paired data for AGB and BGB response to N enrichment in each vegetation type is warranted for identifying the mechanism that can most accurately explain the BGB:AGB ratio decrease caused by N enrichment.

The Northern Hemisphere terrestrial ΔTB caused by N enrichment during 1993–2010 varied among the process-based models simulating terrestrial C cycles with C–N interactions (figure 5). ΔTB was under- or overestimated by most models relative to the estimates from the machine-learning approaches. Different representations of the framework of N cycles in C–N models likely leads to great uncertainty in modeling C cycles (Niu *et al* 2016, Du *et al* 2018). Several key mechanisms of C–N cycles remain to be improved in state-of-the-art terrestrial ecosystem process models, such as community composition, contents of labile C and N, allocation and turnover of C and N pools, biological N fixation, and losses of N from the ecosystem via leaching or gaseous emissions (Thomas *et al* 2015). Our study found that the mismatch between C–N model simulations and observations was widely distributed across Northern Hemisphere terrestrial ecosystems, unlike previous site-scale evaluations of the performance of C–N models (Zaehle *et al* 2014, Dybzinski *et al* 2019). Modeling the effect of N enrichment on Northern Hemisphere terrestrial C cycles in state-of-the-art C–N models should therefore be carefully considered. To more clearly evaluate C–N models' performance, it is essential to conduct in-depth comparative research of observations and model simulations that focuses on N enrichment effect on plant C turnover processes such as growth and mortality of leaf, stem and root. The variables reflecting the characteristics of C turnover across plant organs, therefore, are recommended to be included in the standard output variables of model intercomparison projects.

In summary, our study provided new insights into the quantification of N enrichment impact on Northern Hemisphere plant biomass. N enrichment intensity was the main cause of the S_{AGB} spatial pattern in Northern Hemisphere. N enrichment had a minor effect on Northern Hemisphere terrestrial BGB, indicating that the BGB:AGB ratio decreased as N increased, unlike S_{AGB}. It is worth noting that the machine-learning models do not explain BGB response well (figures 2 and S7), likely due to the lower amount of observational data to constrain the BGB response to N enrichment. This may lead to considerable uncertainty in the ΔTB extrapolation in Northern Hemisphere. Thus, more effort on observing belowground C–N cycling is recommended in future N-enrichment experiments. Given that there is apparent spatial pattern of N limitation of plant growth across global natural terrestrial ecosystems (Du *et al* 2020), the effect of N enrichment on plant growth likely varies across different vegetation types. To accurately quantify the difference in N enrichment effect on AGB and BGB across various ecosystems, it will be useful to conduct more N-enrichment experiments in the ecosystems for which few data are available, such as shrublands, wetland and tundra (table S1). Particularly, long-term N-enrichment experiments are still insufficient (figure S1) but worth carrying out to explore the responses of plant C turnover processes such as mortality (Pregitzer *et al* 2008). Moreover, the components of atmospheric N deposition changed in recent years by increasing reduced N in the United States (Li *et al* 2016) and oxidized N in China (Yu *et al* 2019). The impact on biomass of such changes in the ammonium:nitrate ratio of N deposition remains to be studied in future field experiments.

Data availability statement

The collected records for the response of aboveground and belowground biomass to N enrichment in field experiments were provided as supplementary data in the supplementary information. The gridded Global Soil Dataset for use in Earth System Models (GSDE) was obtained from http://globalchange.bnu.edu.cn/research/soilw

(Shangguan *et al* 2014). WISE30sec database (ISRIC-WISE) data was obtained from http://data.isric.org/geonetwork/srv/eng/catalog.search#/metadata/dc7b283a-8f19-45e1-aaed-e9bd515119bc (Batjes 2016). Global Gridded Soil Phosphorus Distribution Maps data was obtained from https://doi.org/10.3334/ORNLDAAC/1223 (Yang *et al* 2014). The data of global maps of plant traits distribution was obtained from https://github.com/abhirupdatta/global_maps_of_plant_traits (Butler *et al* 2017). Global Mosaics of the standard MODIS land-cover type data product (MCD12Q1) was obtained from https://lpdaac.usgs.gov (Friedl *et al* 2010). Total biomass reported by Carvalhais *et al* (2014) was obtained from www.bgc-jena.mpg.de/geodb/BGI/tau.php. The GEOCARBON global forest AGB was obtained from www.wur.nl/en/Research-Results/Chair-groups/Environmental-Sciences/Laboratory-of-Geo-information-Science-and-Remote-Sensing/Research/Integrated-land-monitoring/Forest_Biomass.htm (Santoro *et al* 2015, Avitabile *et al* 2016). MsTMIP data products were downloaded from https://doi.org/10.3334/ORNLDAAC/1225 (Huntzinger *et al* 2018). Driver data (N deposition) of MsTMIP were downloaded from https://doi.org/10.3334/ORNLDAAC/1220 (Wei *et al* 2014b).

All data that support the findings of this study are included within the article (and any supplementary files).

Acknowledgments

This study was supported by the National Natural Science Foundation of China (42122005, 41701089), and the Youth Innovation Promotion Association CAS (2019074). Funding for the (MsTMIP; https://nacp.ornl.gov/MsTMIP.shtml) activity was provided through NASA ROSES Grant #NNX10AG01A. Data management support for preparing, documenting, and distributing model driver and output data was performed by the Modeling and Synthesis Thematic Data Center at Oak Ridge National Laboratory (ORNL; https://nacp.ornl.gov), with funding through NASA ROSES Grant #NNH10AN681. Finalized MsTMIP data products are archived at the ORNL DAAC (https://daac.ornl.gov). J P was supported by the Spanish Government (Grant PID2019-110521GB-I00), Fundación Ramon Areces (Grant ELEMENTAL-CLIMATE), Catalan Government (Grants SGR 2017-1005), and European Research Council (Synergy Grant ERC-SyG-2013-610028, IMBALANCE-P).

Conflict of interest

The authors declare that they have no conflict of interest.

ORCID iDs

Yongwen Liu https://orcid.org/0000-0002-9664-303X
Shilong Piao https://orcid.org/0000-0001-8057-2292

References

Ackerman D, Millet D B and Chen X 2019 Global estimates of inorganic nitrogen deposition across four decades *Glob. Biogeochem. Cycles* **33** 100–7
Arens S J T, Sullivan P F and Welker J M 2008 Nonlinear responses to nitrogen and strong interactions with nitrogen and phosphorus additions drastically alter the structure and function of a high arctic ecosystem *J. Geophys. Res.* **113** G03S09
Avitabile V *et al* 2016 An integrated pan-tropical biomass map using multiple reference datasets *Glob. Change Biol.* **22** 1406–20
Batjes N H 2016 Harmonized soil property values for broad-scale modelling (WISE30sec) with estimates of global soil carbon stocks *Geoderma* **269** 61–68
Bloom A J, Chapin F S and Mooney H A 1985 Resource limitation in plants—an economic analogy *Annu. Rev. Ecol. Syst.* **16** 363–92
Bradford M A, Fierer N, Jackson R B, Maddox T R and Reynolds J F 2008 Nonlinear root-derived carbon sequestration across a gradient of nitrogen and phosphorous deposition in experimental mesocosms *Glob. Change Biol.* **14** 1113–24
Breiman L 2001 Random forests *Mach. Learn.* **45** 5–32
Butler E E *et al* 2017 Mapping local and global variability in plant trait distributions *Proc. Natl Acad. Sci. USA* **114** E10937–46
Cambui C A, Svennerstam H, Gruffman L, Nordin A, Ganeteg U and Nasholm T 2011 Patterns of plant biomass partitioning depend on nitrogen source *PLoS One* **6** e19211
Canfield D E, Glazer A N and Falkowski P G 2010 The evolution and future of Earth's nitrogen cycle *Science* **330** 192–6
Carvalhais N *et al* 2014 Global covariation of carbon turnover times with climate in terrestrial ecosystems *Nature* **514** 213–7
Chapin F S 1980 The mineral-nutrition of wild plants *Annu. Rev. Ecol. Syst.* **11** 233–60
Chen G S, Yang Y S and Robinson D 2013 Allocation of gross primary production in forest ecosystems: allometric constraints and environmental responses *New Phytol.* **200** 1176–86
Cheng D-L and Niklas K J 2007 Above- and below-ground biomass relationships across 1534 forested communities *Ann. Bot.* **99** 95–102
Craine J M *et al* 2018 Isotopic evidence for oligotrophication of terrestrial ecosystems *Nat. Ecol. Evol.* **2** 1735–44
Dentener F *et al* 2006 Nitrogen and sulfur deposition on regional and global scales: a multimodel evaluation *Glob. Biogeochem. Cycles* **20** GB4003
Du E Z, Terrer C, Pellegrini A F A, Ahlstrom A, van Lissa C J, Zhao X, Xia N, Wu X H and Jackson R B 2020 Global patterns of terrestrial nitrogen and phosphorus limitation *Nat. Geosci.* **13** 221–6
Du Z G, Weng E S, Jiang L F, Luo Y Q, Xia J Y and Zhou X H 2018 Carbon-nitrogen coupling under three schemes of model representation: a traceability analysis *Geosci. Model Dev.* **11** 4399–416
Dybzinski R *et al* 2019 How are nitrogen availability, fine-root mass, and nitrogen uptake related empirically? Implications for models and theory *Glob. Change Biol.* **25** 885–99
Elith J, Leathwick J R and Hastie T 2008 A working guide to boosted regression trees *J. Anim. Ecol.* **77** 802–13

Elser J J et al 2007 Global analysis of nitrogen and phosphorus limitation of primary producers in freshwater, marine and terrestrial ecosystems Ecol. Lett. 10 1135–42
Fick S E and Hijmans R J 2017 WorldClim 2: new 1-km spatial resolution climate surfaces for global land areas Int. J. Climatol. 37 4302–15
Fowler D et al 2013 The global nitrogen cycle in the twenty-first century Phil. Trans. R. Soc. B. 368 20130164
Freschet G T, Violle C, Bourget M Y, Scherer-Lorenzen M and Fort F 2018 Allocation, morphology, physiology, architecture: the multiple facets of plant above- and below-ground responses to resource stress New Phytol. 219 1338–52
Friedl M A, Sulla-Menashe D, Tan B, Schneider A, Ramankutty N, Sibley A and Huang X M 2010 MODIS Collection 5 global land cover: algorithm refinements and characterization of new datasets Remote Sens. Environ. 114 168–82
Galloway J N et al 2004 Nitrogen cycles: past, present, and future Biogeochemistry 70 153–226
Galloway J N, Townsend A R, Erisman J W, Bekunda M, Cai Z C, Freney J R, Martinelli L A, Seitzinger S P and Sutton M A 2008 Transformation of the nitrogen cycle: recent trends, questions, and potential solutions Science 320 889–92
Greaver T L et al 2016 Key ecological responses to nitrogen are altered by climate change Nat. Clim. Change 6 836–43
Gruber N and Galloway J N 2008 An Earth-system perspective of the global nitrogen cycle Nature 451 293–6
Gurevitch J, Koricheva J, Nakagawa S and Stewart G 2018 Meta-analysis and the science of research synthesis Nature 555 175–82
Hedges L V, Gurevitch J and Curtis P S 1999 The meta-analysis of response ratios in experimental ecology Ecology 80 1150–6
Hietz P, Turner B L, Wanek W, Richter A, Nock C A and Wright S J 2011 Long-term change in the nitrogen cycle of tropical forests Science 334 664–6
Huntzinger D N et al 2013 The North American carbon program multi-scale synthesis and terrestrial model intercomparison project—part 1: overview and experimental design Geosci. Model Dev. 6 2121–33
Huntzinger D N et al 2018 NACP MsTMIP: Global 0.5-degree Model Outputs in Standard Format (Oak Ridge, TN: ORNL DAAC)
Janssens I A et al 2010 Reduction of forest soil respiration in response to nitrogen deposition Nat. Geosci. 3 315–22
Kobe R K, Iyer M and Walters M B 2010 Optimal partitioning theory revisited: nonstructural carbohydrates dominate root mass responses to nitrogen Ecology 91 166–79
Lajeunesse M J 2011 On the meta-analysis of response ratios for studies with correlated and multi-group designs Ecology 92 2049–55
LeBauer D S and Treseder K K 2008 Nitrogen limitation of net primary productivity in terrestrial ecosystems is globally distributed Ecology 89 371–9
Li W B, Jin C J, Guan D X, Wang Q K, Wang A Z, Yuan F H and Wu J B 2015 The effects of simulated nitrogen deposition on plant root traits: a meta-analysis Soil Biol. Biochem. 82 112–8
Li Y, Niu S L and Yu G R 2016 Aggravated phosphorus limitation on biomass production under increasing nitrogen loading: a meta-analysis Glob. Change Biol. 22 934–43
Liu Y Y, van Dijk A I J M, de Jeu R A M, Canadell J G, McCabe M F, Evans J P and Wang G J 2015 Recent reversal in loss of global terrestrial biomass Nat. Clim. Change 5 470–4
Makela A, Valentine H T and Helmisaari H S 2008 Optimal co-allocation of carbon and nitrogen in a forest stand at steady state New Phytol. 180 114–23
Mao J et al 2015 Disentangling climatic and anthropogenic controls on global terrestrial evapotranspiration trends Environ. Res. Lett. 10 094008
Mardanov A, Samedovam A and Shirvany T 1998 Root-shoot relationships in plant adaptation to nitrogen deficiency Root Demographics and Their Efficiencies in Sustainable Agriculture, Grasslands and Forest Ecosystems ed J E Box (Dordrecht: Springer) pp 147–54
Müller I, Schmid B and Weiner J 2000 The effect of nutrient availability on biomass allocation patterns in 27 species of herbaceous plants Perspect. Plant Ecol. Evol. Syst. 3 115–27
Niklas K J 2004 Plant allometry: is there a grand unifying theory? Biol. Rev. 79 871–89
Niklas K J 2005 Modelling below- and above-ground biomass for non-woody and woody plants Ann. Bot. 95 315–21
Niu S L et al 2016 Global patterns and substrate-based mechanisms of the terrestrial nitrogen cycle Ecol. Lett. 19 697–709
Ochoa-Hueso R 2016 Nonlinear disruption of ecological interactions in response to nitrogen deposition Ecology 97 2802–14
Peng Y F and Yang Y H 2016 Allometric biomass partitioning under nitrogen enrichment: evidence from manipulative experiments around the world Sci. Rep. 6 28918
Peng Y et al 2022 Globally limited individual and combined effects of multiple global change factors on allometric biomass partitioning Glob. Ecol. Biogeogr. 31 454–69
Peñuelas J et al 2013 Human-induced nitrogen-phosphorus imbalances alter natural and managed ecosystems across the globe Nat. Commun. 4 2934
Peñuelas J, Janssens I A, Ciais P, Obersteiner M and Sardans J 2020 Anthropogenic global shifts in biospheric N and P concentrations and ratios and their impacts on biodiversity, ecosystem productivity, food security, and human health Glob. Change Biol. 26 1962–85
Prager C M et al 2017 A gradient of nutrient enrichment reveals nonlinear impacts of fertilization on Arctic plant diversity and ecosystem function Ecol. Evol. 7 2449–60
Pregitzer K S, Burton A J, Zak D R and Talhelm A F 2008 Simulated chronic nitrogen deposition increases carbon storage in Northern Temperate forests Glob. Change Biol. 14 142–53
Reay D S, Dentener F, Smith P, Grace J and Feely R A 2008 Global nitrogen deposition and carbon sinks Nat. Geosci. 1 430–7
Santoro M et al 2015 Forest growing stock volume of the northern hemisphere: spatially explicit estimates for 2010 derived from Envisat ASAR Remote Sens. Environ. 168 316–34
Schulte-Uebbing L F, Ros G H and de Vries W 2022 Experimental evidence shows minor contribution of nitrogen deposition to global forest carbon sequestration Glob. Change Biol. 28 899–917
Schulte-Uebbing L and de Vries W 2018 Global-scale impacts of nitrogen deposition on tree carbon sequestration in tropical, temperate, and boreal forests: a meta-analysis Glob. Change Biol. 24 E416–31
Shangguan W, Dai Y J, Duan Q Y, Liu B Y and Yuan H 2014 A global soil data set for earth system modeling J. Adv. Model Earth Sys. 6 249–63
Song J et al 2019 A meta-analysis of 1,119 manipulative experiments on terrestrial carbon-cycling responses to global change Nat. Ecol. Evol. 3 1309–20
Stewart G 2010 Meta-analysis in applied ecology Biol. Lett. 6 78–81
Thomas R Q, Brookshire E N J and Gerber S 2015 Nitrogen limitation on land: how can it occur in Earth system models? Glob. Change Biol. 21 1777–93
Tian D S, Niu S L, Pan Q M, Ren T T, Chen S P, Bai Y F and Han X G 2016 Nonlinear responses of ecosystem carbon fluxes and water-use efficiency to nitrogen addition in Inner Mongolia grassland Funct. Ecol. 30 490–9
Tumber-Dávila S J, Schenk H J, Du E Z and Jackson R B 2022 Plant sizes and shapes above and belowground and their interactions with climate New Phytol. (https://doi.org/10.1111/nph.18031)
Viechtbauer W 2010 Conducting meta-analyses in r with the metafor package J. Stat. Softw. 36 1–48

Viechtbauer W, Lopez-Lopez J A, Sanchez-Meca J and Marin-Martinez F 2015 A comparison of procedures to test for moderators in mixed-effects meta-regression models *Psychol. Methods* **20** 360–74

Vitousek P M, Aber J D, Howarth R W, Likens G E, Matson P A, Schindler D W, Schlesinger W H and Tilman D 1997 Human alteration of the global nitrogen cycle: sources and consequences *Ecol. Appl.* **7** 737–50

Wei Y *et al* 2014a The North American carbon program multi-scale synthesis and terrestrial model intercomparison project—part 2: environmental driver data *Geosci. Model Dev.* **7** 2875–93

Wei Y *et al* 2014b *NACP MsTMIP: Global and North American Driver Data for Multi-Model Intercomparison* (Oak Ridge, TN: ORNL DAAC)

Xia J Y and Wan S Q 2008 Global response patterns of terrestrial plant species to nitrogen addition *New Phytol.* **179** 428–39

Xu X T, Liu H Y, Wang W and Song Z L 2018 Patterns and determinants of the response of plant biomass to addition of nitrogen in semi-arid and alpine grasslands of China *J. Arid Environ.* **153** 11–17

Yang X, Post W M, Thornton P E and Jain A K 2014 *Global Gridded Soil Phosphorus Distribution Maps at 0.5-degree Resolution* (Oak Ridge, TN: ORNL DAAC)

You C M, Wu F Z, Gan Y M, Yang W Q, Hu Z M, Xu Z F, Tan B, Liu L and Ni X Y 2017 Grass and forbs respond differently to nitrogen addition: a meta-analysis of global grassland ecosystems *Sci. Rep.* **7** 1563

Yu G R *et al* 2019 Stabilization of atmospheric nitrogen deposition in China over the past decade *Nat. Geosci.* **12** 424–9

Yue K *et al* 2021 Nitrogen addition affects plant biomass allocation but not allometric relationships among different organs across the globe *J. Plant Ecol.* **14** 361–71

Yue K, Fornara D A, Yang W Q, Peng Y, Peng C H, Liu Z L and Wu F Z 2017 Influence of multiple global change drivers on terrestrial carbon storage: additive effects are common *Ecol. Lett.* **20** 663–72

Yue K, Peng Y, Peng C H, Yang W Q, Peng X and Wu F Z 2016 Stimulation of terrestrial ecosystem carbon storage by nitrogen addition: a meta-analysis *Sci. Rep.* **6** 19895

Zaehle S *et al* 2014 Evaluation of 11 terrestrial carbon-nitrogen cycle models against observations from two temperate free-air CO_2 enrichment studies *New Phytol.* **202** 803–22